ELSEVIER

Journal of Non-Crystalline Solids 196 (1996) 297–303

JOURNAL OF NON-CRYSTALLINE SOLIDS

Aggregation model of sonogels on sintering

Nicolás de la Rosa-Fox *, Eduardo Blanco, Luis Esquivias

Departamento de Física de la Materia Condensada (Grupo de Geles), Facultad de Ciencias, Universidad de Cádiz, Aptdo. 40., 11510 Puerto Real, Cádiz, Spain

Abstract

This work presents the application of a geometrical model to dry gels prepared by ultrasonic energy applied to alkoxide–water mixtures (sonogel). The xerogel structure is described as a hierarchical arrangement of spherical units clustered in successive steps. The model takes into consideration the clustering index (number of elementary units in a cluster) and the hierarchical ratio (quotient of cluster to elementary unit size), and accounts for the degree of branching and connectivity along sintering. The structural parameters have been evaluated from small-angle X-ray scattering and gas adsorption data (Brunauer–Emmett–Teller method). The results reveal ultrasonic dose-dependent structural changes on sintering in the 200–900°C temperature range.

1. Introduction

Gels are bi-phased systems (porosity–solid matrix). This porous body sinters by a viscous flow mechanism, causing either pore collapse or coalescence of solid particles [1]. The driving force for this process is supplied by interfacial energy, which works at low temperatures [2].

The interest in sol–gel processing for technological applications is based on the changing gel structure along the successive processing stages, which opens possibilities of tailoring structures for specific applications [3]. Nowadays, tailored porosity represents an important technological need as numerous challenges remain: Engineered porosity below 1 μm, continuous processing methods for nano- and micro-porous materials (e.g., ceramic membranes for gas separation and oxygen transport), defect-free coatings and porous electronic substrates [4–6].

Silica 'sonogels' have particular ultrastructural characteristics on the matter induced by both solventless processing and the cavitation phenomenon, responsible for the alkoxide + water mixture homogenization [7–9]. Monitoring of the structure during gelation by small-angle X-ray scattering (SAXS) informs us that there are two characteristic correlation lengths from which a model of statistic balls can be inferred [10]. These tangles compact during aging giving rise, after drying, to a very homogeneous packing of spheroid particles. This packing is indicated by the wide plateau in the low q-region, presented by the log $I(q)$ versus log q data from a SAXS experiment [11]. In the case of pure silica gels, the size and density of these particles have been estimated to be ~ 1 nm and 2.1 g cm^{-3} from the analysis of wide angle X-ray diffraction data [12]. Consequently, sonogels have a very narrow distribution of pores (~ 2–3 nm), very high bulk density

* Corresponding author. Tel: +34-56 830 966. Telefax: +34-56 837 205. E-mail: rosa@galeon.uca.es.

SSDI 0022-3093(95)00603-6

and surface/volume ratio, two or three times higher than regular gels prepared in alcoholic solution. Homogeneity increases with the ultrasound energy applied and gelling temperature [13].

This work applies a geometric model describing the structure of xerogels as a hierarchical arrangement of clusters in successive steps [14]. An elementary unit a cluster is formed and then, repeating the process, secondary, tertiary, etc., clusters. This approach, on one hand, emphasizes a description of the structure from the 'solid space', as a collection of particles forming clusters with pores within, to the 'pore space', that considers the gel as a collection of voids, more or less interconnected, embedded into a solid backbone [15]. On the other hand, the models described in this paper are a first step toward a connection between both points of view, since our discussion is supported by the surface area of the interface. The link will be done by evaluating the pore volume distribution of these models and comparing them to their experimental counterpart [16,17].

Experimentally, we have different resolution levels, as a consequence of the different sensitivity of SAXS and gas adsorption to evaluate the pore surface area [18]. Thus, from SAXS, we obtain the specific surface area at a level, i. The specific surface area at a level, $i+1$, would be given by means of the BET method, since the finest (or closed) pores are not accessible to the gas. A third level of resolution could be provided by mercury intrusion at atmospheric pressure.

2. Experimental procedures

2.1. Sample preparation and measurements

Silica 'sonogels' were prepared from tetraethoxysilane (TEOS) + water(pH ~ 1) + formamide in a molar ratio of 1:10:7. Formamide is used as a drying control chemical additive (DCCA) in order to obtain monoliths. The liquid mixture was submitted to different energy doses of high power ultrasound (20 kHz): 0.1 kJ cm^{-3} (called **L**) and 0.3 kJ cm^{-3} (called **H**) [13,19]. The sols obtained were kept in hermetically sealed polyethylene containers, gelation taking place at 40°C. After different drying steps below 80°C, monolithic silica xerogels were obtained at 100°C. For the heat treatment, the xerogels were put in a programmable electric furnace and subjected to different isothermal heat treatments at 200, 400, 600, 800 and 900°C in air. A constant heating rate of 1°C/min was used in order to reach the working temperature. Xerogel series were taken, at each temperature, from the same batch in order to have identical structures from the beginning.

The pore analyses were performed in a non-commercial high-vacuum device with nitrogen gas as adsorbate. Pressure was measured with a MKS captor model BHS 1000. Before measuring, the samples were degassed at 100°C in order to empty the pores of physisorbed molecular residuals. The specific surface area was measured using the BET method at relative pressures below 0.35.

Small-angle X-ray scattering experiments were carried out using the LURE synchrotron radiation facility at Orsay, France. A monochromatic beam was selected at 8 keV. The scattered radiation was measured with a one-dimensional position-sensitive detector. Spectra were collected in a range of the scattering vector modulus, $q = 0.01$–0.67 Å^{-1}, $q = (4\pi \sin\theta)/\lambda$, where 2θ is the scattering angle and λ the X-ray wavelength.

2.2. Data analysis

Information coming from gas adsorption can be interpreted on the basis of having an assembly of spheres [20], so that the specific surface area, S, decreases as the particle size, R_s, increases according to the relationship

$$S(\mathrm{m^2 g^{-1}}) = \frac{3 \times 10^4}{R_s(\text{Å})\,\rho_{\text{skeleton}}}, \qquad (1)$$

where the silica spheres have a skeletal density of 2.1 g cm^{-3}.

The SAXS data have been analysed considering the xerogel as a bi-phased media. When positive deviation from Porod's law, due to the electronic density fluctuation on the pore-solid boundary, is observed, it is necessary to consider that $Iq^4 = A + Bq^4$ applies in the high q-region [21]. A is Porod's constant, related to the internal surface-volume ratio. B accounts for the intensity generated by electronic density fluctuations. The contribution of B to the intensity is subtracted from the experimental one in

order to evaluate the integrated intensity, Q_0, and total intensity, Q_1, as

$$Q_0 = \int_0^\infty q^2 I(q)\,\mathrm{d}q \quad \text{and} \quad Q_1 = \int_0^\infty qI(q)\,\mathrm{d}q.$$

The specific surface area may be calculated by the relationship

$$S_{\mathrm{SAXS}} = \pi\Phi(1-\Phi)\frac{A}{Q_0 \cdot \rho_{\mathrm{skeleton}}} \tag{2}$$

where Φ is the solid volume fraction, calculated as the quotient of bulk and skeletal silica densities. The former is calculated by mercury volumetry with an estimated error of 5%, and the latter is taken from the experimental data on vitreous silica (2.2 g cm^{-3}).

The structural parameters were calculated using chord distribution analysis [22]. The xerogel is supposed to be penetrated by random test lines, that makes possible the calculations of the pore chord, R_p, and solid chord, R_s, as the average intersection lengths of the test lines with the voids and solid phases. The mean chord, considering both types of scatterers, is calculated by the relationship

$$R_c = \frac{2}{3}\left(\pi\frac{Q_1}{Q_0}\right). \tag{3}$$

This parameter is the harmonic average of the pore and solid chords, that is

$$\frac{1}{R_c} = \frac{1}{R_s} + \frac{1}{R_p}, \quad \text{being}$$

$$R_s = \frac{R_c}{1-\Phi} \text{ and } R_p = \frac{R_c}{\Phi}. \tag{4}$$

2.3. Aggregation model

The xerogel structure will be made up of elementary spheres of radius, R_s, that form clusters of $R_s + R_p$ average radius [23], from which a hierarchical ratio is calculated as

$$k = \frac{R_s + R_p}{R_s}. \tag{5}$$

The cluster is formed of N elementary spheres. Considering that SAXS and BET data give the specific surface area at two consecutive levels, the relationship [14]

$$\frac{S_{\mathrm{SAXS}}}{S_{\mathrm{BET}}} = \frac{N}{k^2} \tag{6}$$

allows one to calculate an approximate clustering index, N.

The packing fraction is the ratio between the sphere volumes and total cluster volume at this level. The two densities corresponding to the SAXS and BET levels can be calculated from Eq. (1). The packing fractions for each level are related by the relationships

$$\Phi_1 = \frac{\rho_{\mathrm{SAXS}}}{\rho_{\mathrm{skeleton}}}, \quad \Phi_2 = \frac{\rho_{\mathrm{BET}}}{\rho_{\mathrm{SAXS}}}, \quad \Phi_3 = \frac{\rho_{\mathrm{bulk}}}{\rho_{\mathrm{BET}}} \tag{7}$$

which correspond to a hierarchical structure of three levels [15]. The first level (Φ_1) is formed by aggregation of elementary spherical units, the second (Φ_2) corresponds to secondary clusters formed by aggregation of these and the third level (Φ_3) is the macroscopic sample.

Table 1
Experimental parameters of the xerogel series on heating (see text)

Sample [a]	Heat treatment (°C)	$\phi_s \pm 0.01$	$S_{\mathrm{BET}} \pm 5$ (m^{2}g^{-1})	$S_{\mathrm{SAXS}} \pm 5$ (m^{2}g^{-1})	R_c (Å) ±0.5	R_s (Å) ±0.5	R_p (Å) ±0.5
L2	200 (60 min)	0.35	715	437	26	40	74
L4	400 (60 min)	0.32	538	449	28	41	86
L6	600 (60 min)	0.29	592	528	26	37	90
L8	800 (10 min)	0.50	480	497	18	36	36
H2	200 (60 min)	0.31	722	489	24	34	76
H4	400 (60 min)	0.37	620	511	21	34	57
H6	600 (60 min)	0.27	531	491	27	36	98
H8	800 (10 min)	0.51	482	490	18	49	29
H9	900 (10 min)	0.52	395	462	19	53	30

[a] L corresponds to low ultrasonic dose (0.1 kJ cm^{-3}) and H to high ultrasonic dose (0.3 kJ cm^{-3}).

3. Results

Table 1 shows some structural parameters for the xerogel series studied, **L** (low ultrasonic dose) and **H** (high ultrasonic dose). The second column specifies the thermal treatment to which each sample has been submitted. The third column shows the results of the solid volume fraction, the growth of which runs parallel to a decrease in the specific surface area measured by gas adsorption (column 4). That is especially important as it is related to the interfacial energy for the viscous flow on heating. On the other hand, surface areas using Eq. (2) from SAXS data (column 5) show smaller variations.

Columns 6, 7 and 8 (Table 1) show the values from the chord analysis, by means of Eqs. (3) and (4). The results account for the sintering process on heating. The R_c values were calculated taking into account the experimental intensities plotted in Fig. 1. The curve profiles appear with Porod slopes close to -4. However, there is evidence of superimposed single-sphere scattering causing a portion of the curve to have slope < -4 indicated by the inflection around 0.25 Å^{-1}. As can be seen, the results of R_c do not present important variations, in agreement with the regular plateau shown by all samples in the low q-region. In all samples, a little positive deviation from Porod's law can be observed in the high q-region, indicating some roughness of the solid-pore interface.

Note that sample **H** has R_c values less than sample **L**. With regard to R_p, it is worth noting the decrease at 800°C produced by the coalescence of the solid particles. Therefore, the R_s values vary less due to the pore collapse.

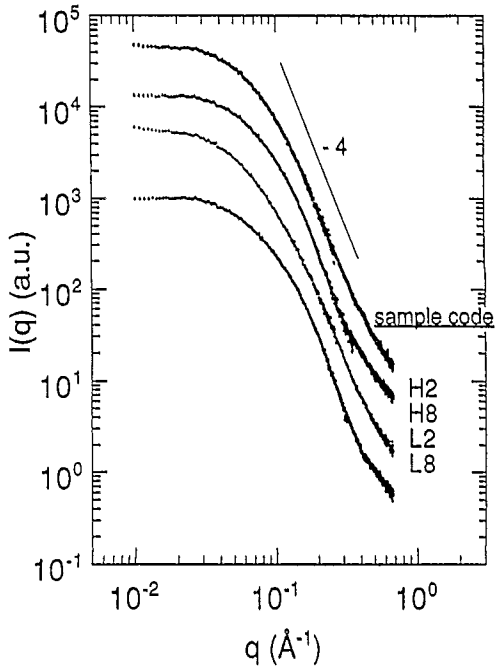

Fig. 1. Log–log plot of SAXS intensities for some of the studied xerogels. H2 and L2 heat treated at 200°C, H8 and L8 at 800°C. The curves were vertically shifted for clarity.

Table 2 shows the calculated hierarchical ratio, k, from Eq. (5) and the clustering index, N, from Eq. (6) for both xerogel series. As can be seen, the k values (column 2) are close to the hierarchical model of hard spheres with real contacts ($k = 3$) [14]. On the other hand, the N values (column 3) increase on heating due to the densification process. For both sample series, maximum packing is produced at 600°C. Over 800°C, this trend breaks, as a conse-

Table 2
Calculate parameters of the xerogels hierarchical structure (see text)

Sample	$k \pm 0.1$	$N \pm 0.5$	ρ_{SAXS} (g cm^{-3}) ± 0.01 [a]	ρ_{BET} (g cm $-^{3}$) ± 0.01 [a]	ρ_{BULK} (g cm^{-3}) ± 0.05
L2	2.9	5	1.73	1.05	0.77
L4	3.1	8	1.65	1.37	0.71
L6	3.5	11	1.56	1.39	0.64
L8	2.0	4	1.65	1.72	1.10
H2	3.2	7	1.79	1.21	0.68
H4	2.7	6	1.75	1.44	0.82
H6	3.7	13	1.68	1.55	0.59
H8	2.7	3	1.72	1.74	1.39
H9	2.8	3	1.76	2.06	1.41

[a] ρ_{SAXS} and ρ_{BET} calculated from Eq. (1).

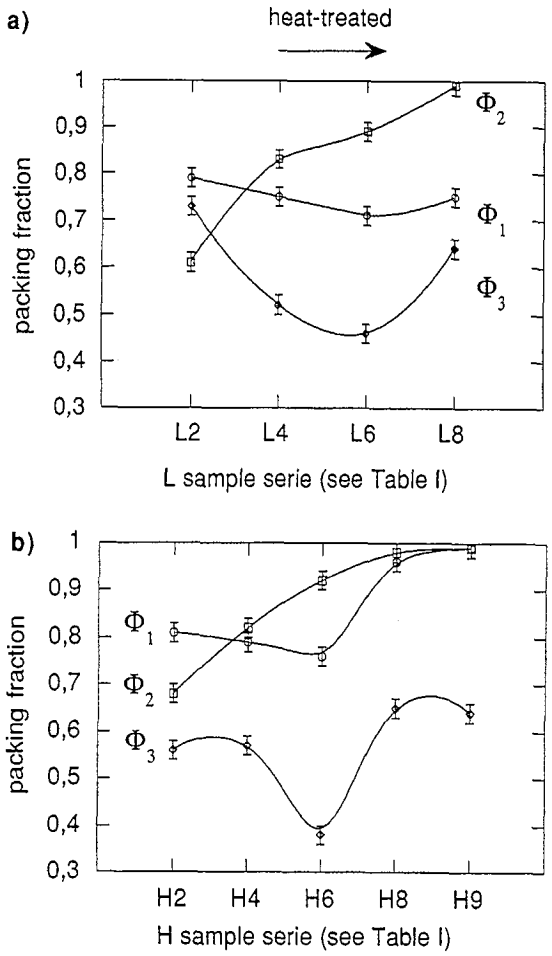

Fig. 2. Calculated packing fractions of the three hierarchical levels as a function of the heat-treatment for (a) sample series, **L**; (b) sample series, **H**. The lines are only a guide to the eye.

quence of the solid phase growth, indicated by the decrease in R_p values. Now the average cluster radius, $R_s + R_p$, is related by R_p in Eq. (5), so the k values decrease and N informs about the loose pore connectivity.

According to Eq. (1), it is possible to calculate the density values at the different resolution levels given by SAXS and BET data (columns 4 and 5). As can be seen, the decrease in the density of the first level runs parallel to an increase in the second one, up to 800°C, when both levels suddenly increase. The density values in column 6 give the bulk density measured by mercury volumetry. It steadily decreases up to 600°C, but clearly rises at 800°C. Fig. 2(a) and (b) showing the behaviour of the packing fractions calculated from Eq. (7) throughout heat treatment (Φ_1, Φ_2 and Φ_3). This provides information about the sintering rate at that level considered.

4. Discussion

Specific surface areas obtained from SAXS data of samples heat-treated at temperatures less than 800°C, are systematically smaller those from BET data in both sample series. A reversed trend is obtained in the samples heat-treated at this temperature. This trend is due to closed porosity and inaccessibility to nitrogen, but the scattering accounts for it. The important decrease in the BET surfaces and the weak variation in the SAXS's indicate that the fore-

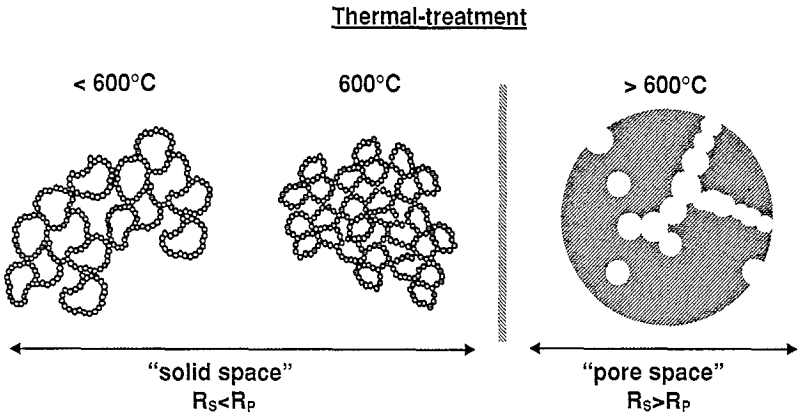

Fig. 3. Schematic structural evolution on sintering accounted for the modeled xerogels, which were obtained by ultrasonic treatment in the sol processes.

most contribution of the interfacial energy for the viscous flow process for sintering is supplied by the second level (Φ_2).

The inflection of log $I(q)$ versus log q (Fig. 1), reflects the spheroidal shape of the scattering centres. This inflection shifts toward lower q-values at 800°C for the heat-treated samples. This fact reveals two aspects: a rough pore-solid boundary and a decrease in the particle size, in agreement with the lower R_c values at this temperature (Table 1).

The sintering process up to 800°C is conducted by a coalescence of the solid particles, increasing their packing fraction Φ_2 (Fig. 2(a) and (b)) [24]. At the same time, this reorganization of the xerogel structure occurs with low packing at the first level (Φ_1), in agreement with the S_{SAXS} small variation (Table 1). This fact produces the formation of some closed porosity, reflected by N fallout.

At temperatures higher than 800°C, the sintering mechanism corresponds to pore collapse. It is worth noting that density (Table 2) and packing fractions (Fig. 2) increase at all levels. In sample, **H**, full density is attained at the first and second levels (Φ_1 and Φ_2). The low packing fraction Φ_3 values indicate the existence of a remaining macroporosity, which needs more interfacial energy due to the short thermal treatment (Table 1).

Fig. 3 shows the sintering process schematically which can be explained as follows. First, at temperatures less than 800°C, the xerogels sinter by coalescence of solid particles and, at higher temperatures, by pore collapse. Similar experimental behaviour results in the same samples submitted to a different thermal treatment that corroborates the hierarchical model presented.

5. Conclusions

The sintering process in xerogels can be modeled as a three-level hierarchical structure formed by the aggregation of elementary silica spheres. Their structure and evolution during sintering are ultrasonic dose-dependent.

At first level (Φ_1) is given by SAXS data, accounting for the rearrangement of the silica spheres. Gas adsorption data reveal the existence of a second level (Φ_2) formed by clusters of the silica spheres. In this intermediate-range structure lies the necessary interfacial energy for viscous flow. At this resolution length-scale, densification forms solid clusters with internal porosity. Sample, **H**, densifies faster than sample, **L**. A third level (Φ_3) corresponds to the xerogel macroscopic structure.

This study features two aspects of the xerogel structure. First, in the low temperature region, the structure is consistent with a description in terms of 'solid space'. The xerogel is made up of entangled spherical particles, which coalesce to form ramified secondary clusters. Second, in the high temperature region, the structure is better depicted as 'pore space' because of the presence of closed pores, the collapse of which yields the final silica glass.

Acknowledgements

This work has been supported by the Spanish ICI (Instituto de Cooperación Iberoamericano) and the Plan Andaluz de Investigación (PA-6015) of the Andalusian government.

References

[1] C.J. Brinker and G.W. Scherer, in: Sol–Gel Science: The Physics and Chemistry of Sol–Gel Processing (Academic Press, San Diego, 1990) ch. 11.
[2] J. Zarzycki, in: Glasses and the Vitreous State (Cambridge University, Cambridge, 1991) ch. 18.
[3] L.C. Klein, Sol–gel Technology for Thin Films, Fibers, Preforms, Electronics and Speciality Shapes (Noyes, New Jersey, 1988).
[4] L.L. Hench and J.K. West, Chem. Rev. 90 (1990) 33.
[5] D.W. Schaefer, Mater. Res. Soc. Bull. XIX (4) (1994) 14.
[6] D.M. Smith, D-W Hua and W.L. Earl, Mater. Res. Soc. Bull. XIX (4) (1994) 44.
[7] N. de la Rosa-Fox, L. Esquivias and J. Zarzycki, Diff. Defect Data 53&54 (1987) 363.
[8] N. de la Rosa-Fox, L. Esquivias and J. Zarzycki, J. Mater. Sci. Lett. 10 (1991) 1237.
[9] D. Levy and L. Esquivias, Adv. Mater. 7 (1995) 120.
[10] M. Ramirez-del-Solar, L. Esquivias, A.F. Craievich and J. Zarzycki, J. Non-Cryst. Solids 147&148 (1992) 206.
[11] N. de la Rosa-Fox, L. Esquivias, A.F. Craievich and J. Zarzycki, J. Non-Cryst. Solids 121 (1990) 211.
[12] M.C. Barrera-Solano, N. de la Rosa-Fox and L. Esquivias, J. Non-Cryst. Solids 147&148 (1992) 194.
[13] E. Blanco, N. de la Rosa-Fox, L. Esquivias and A.F. Craievich, J. Non-Cryst. Solids 147&148 (1992) 296.

[14] J. Zarzycki, J. Non-Cryst. Solids 121 (1990) 110.
[15] J. Zarzycki, J. Non-Cryst. Solids 147&148 (1992) 176.
[16] J. Zarzycki, in: Chemical Processing of Advanced Materials, ed. L.L. Hench and J.K. West (Wiley, New York, 1992) p. 77.
[17] J. Rodríguez-Ortega and L. Esquivias, presented at the 7th Int. Workshop on Glasses and Ceramics from Gels, Sept. 18–22, 1995, Faro, Portugal.
[18] K.A. Hardman-Rhyne, in: Advanced in Ceramics, Vol. 21: Ceramic Powder Science (American Ceramic Society, New York, 1987) p. 767.
[19] E. Blanco, R. Litrán, M. Rámirez-del-Solar, N. de la Rosa-Fox and L. Esquivias, J. Mater Res. 9 (11) (1994) 2873.
[20] R.K. Iler, The Chemistry of Silica (Wiley, New York, 1979) ch. 5.
[21] W. Ruland, J. Appl. Crystallogr. 4 (1971) 70.
[22] G. Porod, in: Small Angle X-Ray Scattering, ed. O. Glatter and O. Kratky (Academic Press, London, 1982) p. 17.
[23] D.E.G. Williams, Philos. Mag. B50 (3) (1984) 363.
[24] M. Ramírez-del-Solar and L. Esquivias, J. Sol–Gel Sci. Tech. 3 (1994) 41.